IEEE Access
Multidisciplinary | Rapid Review | Open Access Journal

Received January 23, 2021, accepted February 7, 2021, date of publication February 10, 2021, date of current version February 24, 2021.

Digital Object Identifier 10.1109/ACCESS.2021.3058352

A Low-Profile Dielectric Resonator Antenna With Compact-Size and Wide Bandwidth by Using Metasurface

SHU-KUAN ZHAO[1], NENG-WU LIU[1], (Member, IEEE), QIANG CHEN[2], (Senior Member, IEEE), GUANG FU[1], AND XIN-PENG CHEN[1]

[1]Science and Technology on Antenna and Microwave Laboratory, Xidian University, Xi'an 710071, China
[2]Electromagnetic Engineering Laboratory, Tohoku University, Sendai 980-8579, Japan

Corresponding authors: Neng-Wu Liu (yb47448@umac.mo) and Guang Fu (gfu@mail.xidian.edu.cn)

This work was supported in part by the National Natural Science Foundation of China under General Program under Grant 61801348, in part by the Shaanxi Province Program under Grant 2018022, and in part by the National Natural Science Foundation of Shaanxi Province under Grant 2019JM-201.

ABSTRACT A dielectric resonator antenna (DRA) with the loading of metasurface (MS) is proposed for low-profile, wide-bandwidth and compact-size. Firstly, an MS structure consisting of 6×6 periodic metallic patch cells is loaded above the DRA. It aims to excite an additional TM surface wave above the fundamental TE_{111} mode of the rectangular DRA. Then, the shorting walls are printed on two sides of the dielectric, thus moving down the operating frequency with respect to its TM surface wave mode. As such, the bandwidth of the antenna is significantly widened with compact-size under the operation of TE_{111} and TM surface wave modes. Finally, the proposed DRA with enhanced performance is fabricated and tested. The results show that an impedance bandwidth of the antenna is dramatically increased to about 17.2%, covering the frequency range from 1.75 to 2.08 GHz, which is about 9.6 times wider than the traditional DRA at the same thickness (1.8%). Besides, it still maintains the broadside radiation pattern with stable gain of around 6.6 dBi and fairly low cross polarizations of below -26 dB. Particularly, the overall size of the radiator still maintains as small as about $0.32\lambda_0 \times 0.32\lambda_0 \times 0.044\lambda_0$. It should be noted that the analysis of the antenna is carried out by using Ansys HFSS software version 14.0 and ADS 2011.

INDEX TERMS Dielectric resonator antenna (DRA), compact size, wide-bandwidth, low-profile, metasurface.

I. INTRODUCTION

Since it was first put forward in the early 1980s [1], the dielectric resonator antennas (DRAs) have drawn considerable attention due to its several attractive features, i.e., high radiation-efficiency, small size, and high design freedom [2]–[5]. Unfortunately, the traditional DRA has a major drawback of limited bandwidth as well as the microstrip antenna, especially in a low-profile condition. As such, the low-profile DRA is not suitable for many wideband applications [6].

During the past two decades, several attempts have been made to investigate and address the drawback of the inherent narrow bandwidth. Firstly, a variety of DRAs with special shapes were proposed to lower the Q-factor and hence increase their impedance bandwidths. In [7] and [8], inverted stepped pyramidal shape and T-shape were introduced to achieve a wideband property of more than 60%. However, this approach increased the design complexity or profile of the DRAs. In addition, the peculiar shapes also led to the high cross-polarization of about -9dB. Secondly, the DRAs with high aspect ratio using different excitation methods were applied to merge the dominant mode with higher order modes. In [9] and [10], although their bandwidths were kept above 45%, these antennas had the overall thickness of more than $0.25\lambda_0$ (λ_0 is the free-space wavelength). In [11], a pair of vertical microstrip lines was used in a perpendicular arrangement to excite the cylindrical dielectric resonator antenna for circularly polarized performance. Two resonances offered an axial ratio bandwidth of 24.6%, but the

The associate editor coordinating the review of this manuscript and approving it for publication was Wanchen Yang.

This work is licensed under a Creative Commons Attribution 4.0 License. For more information, see https://creativecommons.org/licenses/by/4.0/

high profile of $0.24\lambda_0$ was still maintained. Thirdly, different resonators could be combined with DRAs to form multi-resonant hybrid antennas. In [12] and [13], a slot and a patch were utilized to introduce additional resonances and widen their bandwidths to about 25% and 21.3%, respectively. Unfortunately, these DRAs also suffered from several critical issues, such as high profile, large transverse dimensions or low gain. Fourthly, the DRAs with different permittivities could be vertically stacked with each other to provide excellent broadband performance. Impedance bandwidths to about 40% or even wider were achieved in [14], [15]. Nevertheless, these stacked DRAs had high profile, high cross-polarization or asymmetrical radiation pattern. According to these previous methods of realizing broadband DRA, little attention was simultaneously paid to the size-reduction of the 3-D antenna geometry and stable broadside radiation, thus achieving desired compact-size and wide-bandwidth. In recent years, the metasurface (MS) has been used to design new types of antennas with improved performance, such as broadband and compact size. In [16], a rectangular and semicircular patch separated by a gap was intended to arouse zeroth-order resonance mode. The antenna realized a bandwidth of 23.64% with a compact size of $0.276\lambda_0 \times 0.129\lambda_0$. In [17], the MS was loaded on a patch antenna to generate additional resonances, and its axial-ratio bandwidth is extended to about 23.4%.

In this paper, a dielectric resonant antenna with compact geometry and enhanced bandwidth is proposed. The MS structure is introduced to reduce the profile of the antenna and generate an extra resonance of the TM surface wave mode. Furthermore, a pair of shorting conducting walls are used to decrease the resonant frequency of the MS aiming to realize the wide-bandwidth characteristic. The proposed antenna is numerically studied and related measurements are carried out to verify working principles and simulated results.

II. GEOMETRY AND WORKING PRINCIPLE

A. DRA CONFIGURATION

The configuration and parameters of the proposed DRA are depicted in Fig. 1. It consists of the MS (top layer), the DR (middle layer), the aperture-coupled ground plane, and the microstrip feeding line (bottom layer). For the MS, it is etched on the top side of Rogers 4350B substrate ($\varepsilon_r = 3.66$ and tan $\delta = 0.004$) in Fig. 1 (b). For the rectangular DR ($\varepsilon_r = 15$ and tan $\delta = 0.0015$), it is loaded underneath the MS in Fig. 1(c). For the 50Ω microstrip feeding line, it is placed at the bottom surface of F4BM substrate ($\varepsilon_r = 2.2$ and tan $\delta = 0.0009$). In addition, a pair of shorting walls is inserted on two sides of the dielectric along the y-axis. Due to the etched slot on the ground along y-axis, only these odd-order modes could be successfully generated in the DRA [18].

B. IMPEDANCE BANDWIDTH ENHANCEMENT OF THE ANTENNA

The TE modes of the dielectric resonant antenna (RDRA) under aperture coupling are deeply investigated in [19].

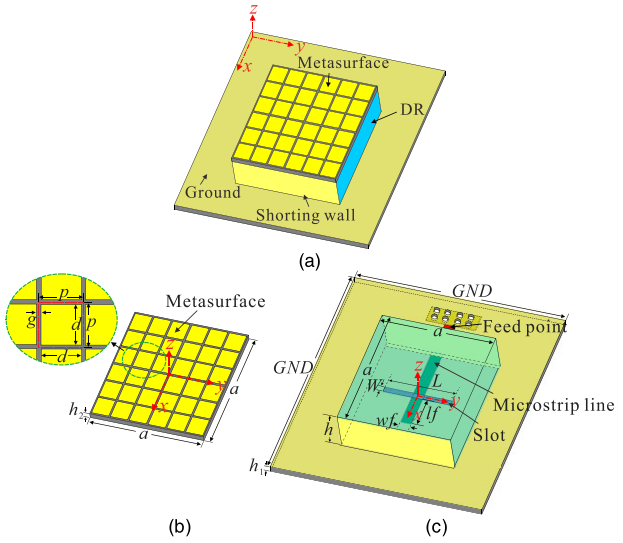

FIGURE 1. Configuration of the proposed DRA. (a). 3-D view. (b). Metamaterial structure. (c). Feeding structure and DR.

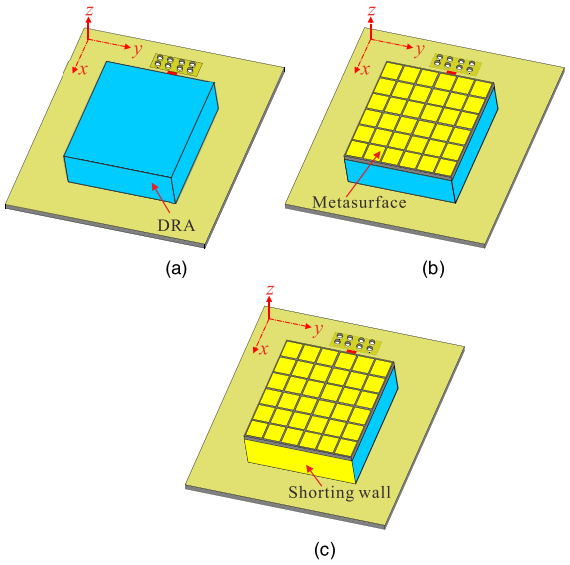

FIGURE 2. Evolution process of our proposed DRA with bandwidth enhancement and miniaturization. (a). Reference antenna 1, (b). Reference antenna 2 with the MS, (c). Proposed DRA with the MS and the shorting walls.

The specific mode can be represented by TE^{y}_{mnp}, where the superscript y represents that the component of E-field in the y-direction is 0. Meanwhile, the value of m, n, and p respectively represent the field variation along x-, y- and z-axis. To explain the working principle of our proposed antenna clearly, two reference antennas are compared. Firstly, selecting a rectangular DR with the same size as the reference antenna 1 is shown in Fig. 2(a). Secondly, loading the MS on the DR to reduce profile as reference antenna 2 is depicted in Fig. 2(b). Thirdly, inserting a pair of shorting walls on two sides of the dielectric to reallocate the resonant frequencies. Finally, the proposed DRA with improved performance is realized in Fig. 2(c).

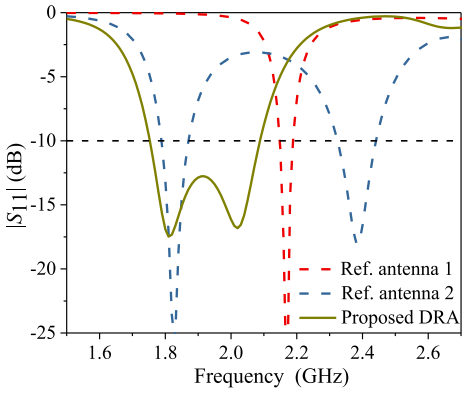

FIGURE 3. Simulated $|S_{11}|$ of the reference DRAs and our proposed DRA.

TABLE 1. Dimensions of the proposed DRA (Unit: mm).

Design parameters	h	h_1	h_2	a	W	L
Value(mm)	7	1.016	0.254	50	1	21
Design parameters	wf	lf	p	d	g	GND
Value (mm)	3.12	12.2	8.2	8	0.2	95

Fig. 3 depicts the simulated $|S_{11}|$ of the reference antennas and proposed DRA. As expected, the single-mode dielectric resonator of the reference antenna 1, especially in the low-profile condition, suffers from a narrow bandwidth (1.8%). To solve this inherent issue, the MS structure is employed in the reference antenna 2. A new resonance is generated, but the broadband characteristics of the antenna are still not realized. Finally, the shorting walls are loaded around the DR to reallocate two resonances in proximity to each other. Relying on these approaches, the impedance bandwidth of the designed DRA is significantly extended to 17.2%, which is about 9.6 times wider than the traditional DRA under the same small thickness (1.8%). The mechanism of this phenomenon will be discussed in the following.

C. WORKING MECHANISM OF THE ANTENNA

The reallocation of multiple radiative modes to enhance the impedance bandwidth is applied to our proposed antenna [20]. The dielectric waveguide model (DWM) can be utilized to calculate the resonant frequency of the traditional rectangular dielectric resonant antenna (RDRA) [21]. The resonant frequency of $TE_{111}{}^{y}$ mode can be expressed as:

$$f_{DR} = \frac{c}{\lambda\sqrt{\varepsilon_r}} = \frac{ck_0}{2\pi\sqrt{\varepsilon_r}} \tag{1}$$

$$k_0 = \sqrt{k_x^2 + k_y^2 + k_z^2}, \quad k_x = \frac{\pi}{a}, \; k_z = \frac{2\pi}{h} \tag{2}$$

$$k_y \tan(\frac{ak_y}{2}) = \sqrt{k_x^2 + k_z^2} \tag{3}$$

where k_x, k_y, and k_z are the wavenumbers along the x-, y-, and z-directions, respectively. Here, c is the speed of light and k_0 is the free-space wavenumber.

TABLE 2. Resonant frequencies of the DR under different dimensions.

(a,h)(mm)	(50,12)	(50,12.85)	(50,14)	(40,12)	(60,14)
f_{DWM}(GHz)	1.89	1.80	1.69	2.02	1.61
f_{HFSS}(GHz)	1.82	1.73	1.65	1.94	1.55
Error (%)	3.7	3.8	2.3	2.9	3.7

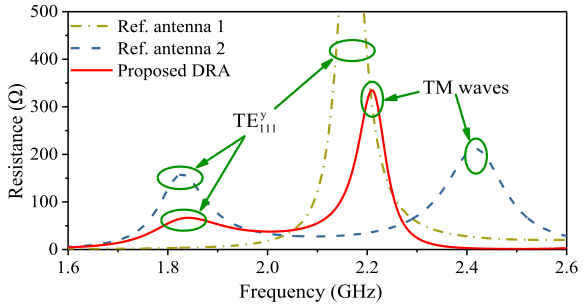

FIGURE 4. Migration of resonant frequencies of TE_{111}^{y} and TM waves under three DRAs with different structures.

Table 2 displays the fundamental mode resonant frequencies of the DRA obtained from the DWM and full-wave simulation under different sizes, indicating that the error between the theoretical calculations and the full-wave simulation results is less than 4%. However, the final dimensions of the DR cannot be determined directly due to the loading of MS. The initial height of the DR can be provisionally determined first, and on this basis, the design of the MS can be carried out. Here, reference antenna 1 with the thickness of 7mm is chosen as the starting point of the design. The relevant resistance curves are shown in Fig. 4. Seeing that the fundamental mode $TE_{111}{}^{y}$ of the reference antenna 1 with the feed structure is excited around 2.17 GHz. Besides, in the reference antenna 2, TM surface wave propagating on the MS is excited to provide an additional radiative mode. In other words, it provides preconditions for broadening the antenna bandwidth.

It is well-known that the reflection phase diagrams are usually used to investigate the resonance characteristics of the MS. As depicted in Fig. 5(a), the simulated model of the unit cell is adopted for numerically computing the reflection phase of the MS. Based on the proposed dimensions, the zero-degree reflection phase occurs at 1.8GHz with reference to Fig. 5(b). Further, the analysis method of surface wave resonances in [17] is introduced. The resonances of the surface modes can be qualitatively determined by the following equations:

$$\beta_{sw} = \frac{\pi}{L_{ms}} = \frac{\pi}{N \times p} = \frac{\pi}{N \times (d+g)} \tag{4}$$

$$\frac{360^\circ}{\pi} \cdot \beta_{sw} \mathrm{p} = \frac{360^\circ}{N} \tag{5}$$

where β_{sw} is the propagation constant of the above-mentioned surface waves, and L_{ms} is the total length of the MS. The number of patch cells and the periodicity of the MS are N and p, respectively.

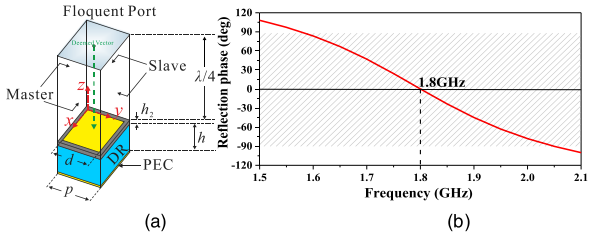

FIGURE 5. (a). Simulated model of the MS unit cell. (b). Reflection phase based on the proposed dimensions.

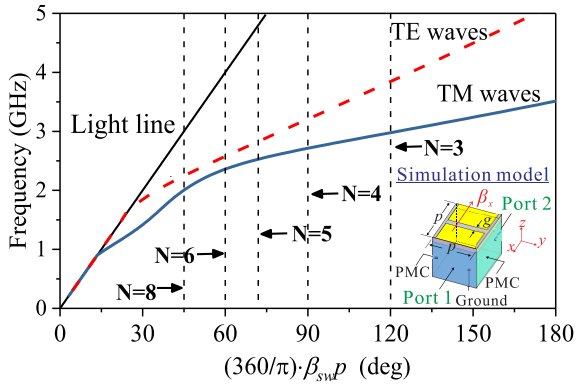

FIGURE 6. Dispersion diagram of the unit MS scheme and graphic solutions of (2) under different numbers of the unit cell.

TABLE 3. Resonant frequencies of TM surface wave under different numbers of unit cells.

Configuration	3×3 cell	4×4 cell	5×5 cell	6×6 cell	8×8 cell
f_{TM} (GHz)	2.98	2.72	2.51	2.36	2.01

According to the simulated results from (4) upon the boundary condition, the dispersion diagram of the MS is plotted in Fig. 6. The resonant frequencies of surface wave modes can be precisely demonstrated by the intersections in terms of the dispersion curves and vertical lines representing the value on the right side of (5). Table 3 summarizes the resonances of the TM surface wave mode obtained by the full-wave approach for the MS with different cell numbers. The results depict that the number of MS units has significant effects on the surface wave resonances. Therefore, the appropriate number of cells should be selected purposefully to improve the antenna performance. For N = 6, the resonant frequency for the TM surface wave is 2.36 GHz. This frequency is close to the resonant frequency of the DRA mode as mentioned before, so the MS structure of 6 × 6 is applied to yield wide bandwidth. The real impedance curve of the reference antenna 2 on this occasion is shown in Fig. 4. The resonant frequency of the additional TM surface wave is 2.42 GHz, which is approximately consistent with the data extracted from Table 3.

Benefit from the miniaturized impact of the MS, the resonant frequency of the fundamental mode (TE^{y}_{111} mode) of the DRA is decreased from 2.17 GHz to 1.83 GHz, as compared with the reference antenna 1. To further explain the principle

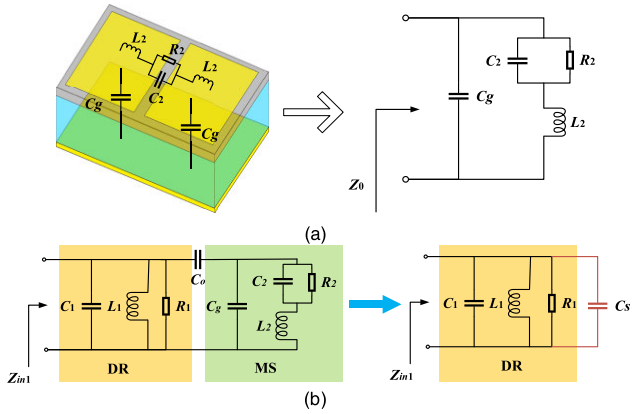

FIGURE 7. Equivalent circuits of (a) the MS and (b) the reference antenna 2.

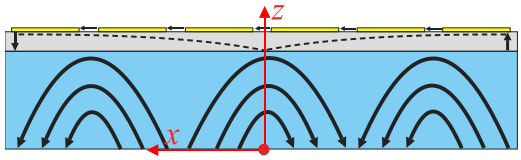

FIGURE 8. Sketch of the *E*-field distribution of reference antenna 2 with MS over xoz-plane at 2.42GHz.

of antenna miniaturization, the equivalent circuit model of the MS and the reference antenna 2 is given in Fig. 7. The traditional DRA can be simplified to a RLC parallel circuit, and the resonant frequency of the DRA is determined by:

$$f_1 = \frac{1}{2\pi}\frac{1}{\sqrt{L_1 C_1}} \tag{6}$$

Then, a new equivalent RLC circuit is added by the MS to generate a new resonance. At the same time, the MS provides an additional load for low frequency resonance. In this state, the MS structures can be further equivalent to a capacitor *Cs*, as shown in Fig.7(b), and its resonant frequency of the fundamental mode of the DRA can be further expressed by:

$$f_2 = \frac{1}{2\pi}\frac{1}{\sqrt{L_1(C_1 + C_s)}} \tag{7}$$

The larger capacitance implies the lower resonant frequency of the DR. Obviously, the loading of the MS excites a new resonance and reallocate the fundamental mode of the DRA. Unfortunately, the distance between the two radiative modes is still too far to realize a broad impedance bandwidth.

Then, our main target is to further merge these two modes, aiming to construct a compact wideband DRA under dual-resonance. To clarify the working mechanism more in detail, the sketch of the *E*-field of the reference antenna 2 with the MS loaded is illustrated in Fig.8. The $TE_{311}{}^{y}$ mode is excited in the DRA at 2.42 GHz. Due to the utilization of the dielectric resonator with high dielectric constant, the interfacial surface between the dielectric and air is regarded as a magnetic plane, and the normal component of the electric

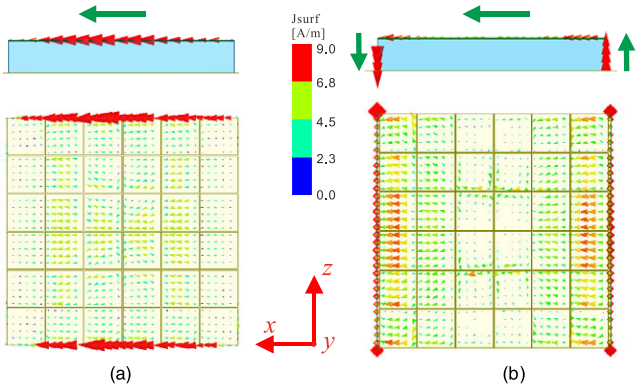

FIGURE 9. Simulated surface currents distribution of the antenna at 2.21 GHz. (a). Reference antenna 2. (b). Proposed antenna.

field on its surface is zero. Based on the electric-field distribution, a pair of shorting walls are loaded on both sides of the DR parallel to the *y*-axis, as shown in Fig. 2(c). Fig.4 shows that the resonant frequency of TM surface wave resonance is decreased from 2.42 GHz to 2.21 GHz, in other words, the electrical size of the MS decreases, whereas that of TE_{111}^{y} mode is basically unchanged. To identify the reasons for this phenomenon, the current distribution of the antenna with and without the shorting walls at 2.21 GHz are presented in Fig. 9. The horizontal current is produced by the MS, indicating the high frequency resonance of the antenna is sensitive about the number of unit cells. The vertical current is induced on the shorting walls by the *E*-field produced by the horizontal current on the MS. The extension of the current path causes the bandwidth of the MS to shift to lower frequencies. Finally, the reallocation of these dual modes leads to the desired broadband performance.

D. MODES AND CIRCUIT ANALYSIS OF THE ANTENNA

To verify the operating modes of the antenna, the simulated *E*-field distributions of the antenna are presented. The *E*-field distributions at *xy*-plane are demonstrated in Fig. 10 at the resonant frequency of 2.21GHz. It is clear that the electromagnetic (EM) waves are radiated from the edge slots of the metasurface along the x-direction (*E*-plane), indicating the resonance operates at a TM surface wave mode as demonstrated in [22]. The sketch and simulated results of the *E*-field distributions of the proposed antenna at *xy*-plane are plotted in Fig.11, which demonstrates that the low resonance is TE_{111}^{y} mode of the DR and the other one is TM_{10} surface wave mode of the MS. The in-phase radiated field distribution are excited in both resonances. Therefore, a stable normal radiation pattern with identical polarization can be maintained over the entire operating bandwidth.

Finally, the entire equivalent circuit of the antenna is constructed to verify the design principle. The circuit and parameters are presented in Fig. 12. The impedance transformers with turn ratios equal to n_1 and n_2 are configured to describe the couplings of the aperture to the microstrip line and the DRA to the aperture, respectively [23]. Then,

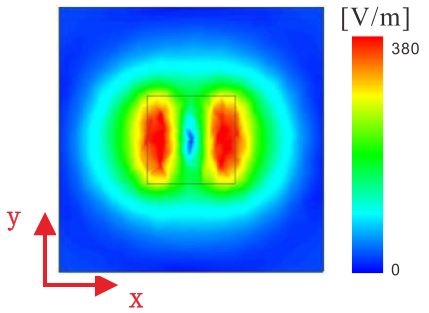

FIGURE 10. Amplitude distribution of *E*-field of the proposed DRA at 2.21GHz. xy-plane, z = 15mm.

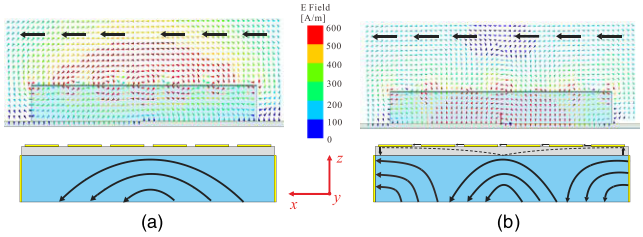

FIGURE 11. *E*-field distributions of the proposed DRA over the xoz-plane. (a). Proposed antenna at 1.84 GHz. (b). Proposed antenna at 2.21 GHz.

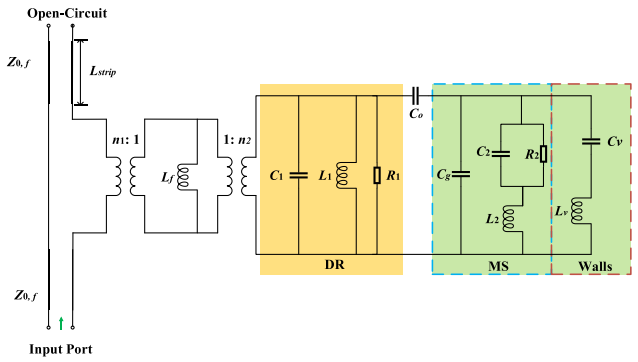

FIGURE 12. Equivalent circuit model of the proposed DRA. ($Z_{o,f}$ = 50 Ω, L_{strip} = 12.7mm, n_1 = 9.4, n_2 = 4.3, L_f = 87.94 nH, C_1 = 0.03 pF, L_1 = 6.72 nH, R_1 = 527 Ω, C_o = 14.29 pF, C_g = 0.1 pF, C_2 = 0.73 pF, R_2 = 822 Ω, L_2 = 9.32 nH, C_v = 2.41 pF, L_v = 4.32 nH).

two RLC circuits connected in series through the coupling capacitor C_o demonstrate the resonances of DR and MS separately. Finally, the capacitance C_v introduced by the coupling of the MS and the shorting walls and the L_v introduced by the grounded shorting walls are set in parallel with the RLC circuit of the MS. The simulated $|S_{11}|$ obtained by the ADS is given in Fig. 14, indicating good agreement with the full-wave simulation over the entire operating bandwidth.

E. DESIGN GUIDELINE

Based on the above-mentioned working mechanism, a design guideline is suggested finally. It is assumed that the lower and upper frequency resonances of the antenna are f_1 and f_2, respectively.

Step 1: Calculating the dimensions of the DR based on the DWM at f_1.

TABLE 4. Performance comparison between our proposed DRA and other previous DRAs.

Refs	Methods	Profile	Transverse dimension	BW(%)	Pattern symmetry	Peak cross-pol	Gain (dBi)
[7][8]	Special shape	$0.09\lambda_0$↑ $0.26\lambda_0$↑	$0.28\lambda_0 \times 0.28\lambda_0$ $0.14\lambda_0 \times 0.49\lambda_0$↑	62.0% 75.1%	yes no	NG ~-9dB↑	~6.5 3.27-7.35↓
[9][10][11]	High aspect ratio	$0.25\lambda_0$↑ $0.39\lambda_0$↑ $0.24\lambda_0$↑	$0.11\lambda_0 \times 0.23\lambda_0$ $0.29\lambda_0 \times 0.29\lambda_0$ $0.11\lambda_0 \times 0.11\lambda_0$	62% 46% 24.6%	no yes yes	~-20dB↑ ~-20dB↑ ~-18dB↑	5.5-9.5 ~6.2 ~5.5↓
[12][13]	Hybrid structure	$0.13\lambda_0$↑ $0.18\lambda_0$↑	$0.22\lambda_0 \times 0.22\lambda_0$ $1.09\lambda_0 \times 1.09\lambda_0$↑	25% 21.3%	no yes	~-25dB ~-28dB	2.8-4.5↓ ~9
[14][15]	Stacked DR	$0.35\lambda_0$↑ $0.09\lambda_0$↑	$0.28\lambda_0 \times 0.18\lambda_0$ $0.76\lambda_0 \times 0.76\lambda_0$↑	103% 40%	no yes	~0dB↑ ~-30dB	~6↓ ~9
Traditional DRA in Fig. 2 (*a*)	Single mode	$0.044\lambda_0$	$0.32\lambda_0 \times 0.32\lambda_0$	1.8%	yes	-47dB	5.7↓
Our work	**Hybrid structure**	**$0.044\lambda_0$**	**$0.32\lambda_0 \times 0.32\lambda_0$**	**17.2%**	**yes**	-26dB	**~6.6**

NG: not giving; λ_0: wavelength at the center frequency of the operating band; BW: bandwidth

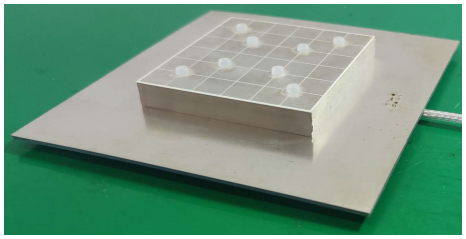

FIGURE 13. Photograph of the proposed DRA.

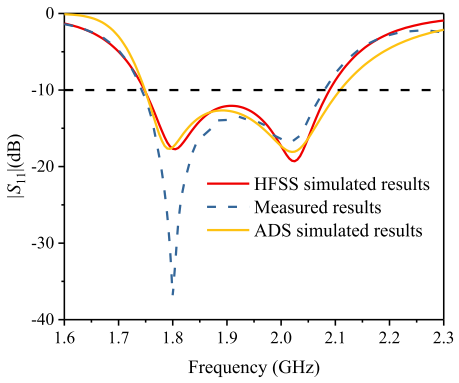

FIGURE 14. Simulated and measured $|S_{11}|$ of the proposed DRA.

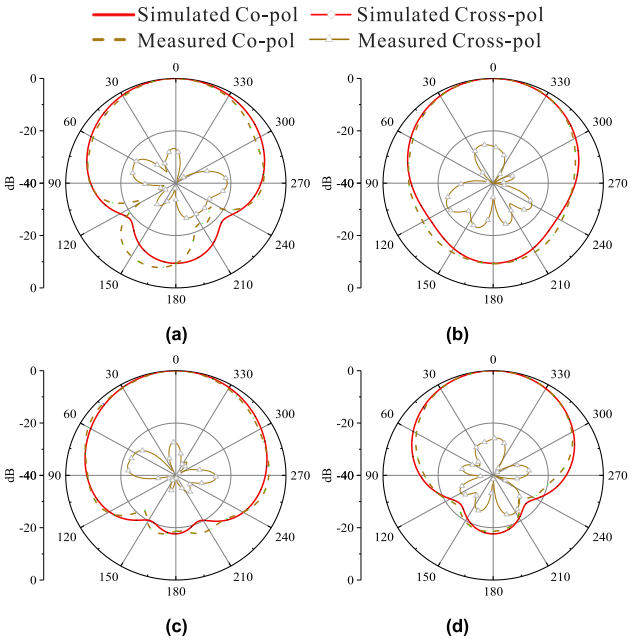

FIGURE 15. Simulated and measured radiation patterns of the proposed antenna. (a). xoz-plane, 1.8GHz. (b). yoz-plane. 1.8GHz. (c). xoz-plane, 2.02GHz. (d). yoz-plane, 2.02GHz.

Step 2: Setting the initial height of the DR, and optimize the dimensions and the number of the MS unit cells according to the resonant frequency of the TM surface wave, i.e. f_2.

Step 3: Setting the transverse size of DR to match the size of the MS. Simulate the model to achieve the dual resonance performance of the antenna.

Step 4: Inserting a pair of the shorting walls on two sides of the DR to reallocate the two resonances for the desired broadband performance.

It should be noted that the steps 2 to 4 herein need to be debugged repeatedly to achieve optimal results.

III. EXPERIMENTAL RESULTS AND DISCUSSIONS

To demonstrate the improved performance from simulated results, a prototype of the proposed DRA with the MS and shorting walls loaded is fabricated and tested. Fig. 13 presents the assembled prototype of the antenna.

Firstly, the reflection coefficient ($|S_{11}|$) of the antenna is measured by utilizing the AV3672B vector network analyzer and depicted in Fig. 14. The measured $|S_{11}|$ with two attenuation poles (1.80 and 2.02GHz) is consistent with the simulated one (1.81 and 2.03 GHz). As a result, the measured bandwidth of the antenna for $|S_{11}| < -10$ dB is significantly extended to about 17.2% (1.75–2.08 GHz), which is about 9.6 times wider than the traditional counterpart at the same thickness (1.8%). It is worth pointing out that the desired wide-bandwidth is acquired with a compact size of $0.32\lambda_0 \times 0.32\lambda_0 \times 0.044\lambda_0$.

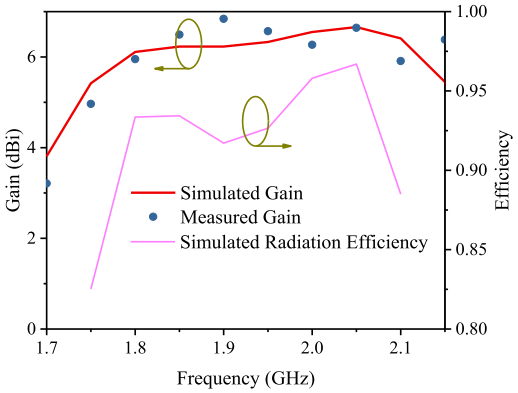

FIGURE 16. Simulated and measured peak gains and radiation efficiency of the proposed DRA.

Secondly, the radiation pattern is tested by using a near-field SATIMO antenna test system. Fig. 15 plots the measured and simulated radiation patterns at 1.8 GHz and 2.0 GHz. It is clear that the measured results are in line with the simulation. At the same time, a stable normal radiation pattern with identical polarization and low cross-polarization properties is satisfactorily achieved under the operation of desired dual radiative resonant modes. Fig. 16 depicts the realized gain and the radiation efficiency of the proposed antenna. It can be seen that stable radiation with the peak realized gain of about 6.6 dBi and the radiation efficiency of about 92% is satisfactorily attained in the operating bandwidth.

In the end, a detailed comparison between our designed DRA and previous attractive works [7]–[14] is tabulated in Table 4. Generally speaking, the proposed antenna has low profile and compact transverse dimensions, while yielding a wide impedance bandwidth and good radiation properties.

IV. CONCLUSION

In this paper, a miniaturized broadband dielectric resonant antenna is proposed under dual-mode resonance. Firstly, periodic metallic patch cells are loaded on the rectangular DRA for miniatured size, while the surface wave of MS is also excited to generate additional resonances. Secondly, a pair of shorting conducting walls is introduced to reduce the resonant frequency of TM surface wave mode, whereas keeping the resonant frequency of the DR almost unchanged. Relying on these methods, the desired dual resonant modes are merged with each other, achieving an improved impedance bandwidth. The measured results are matched well with the simulation, achieving a broad impedance bandwidth of about 17.2% with the identical polarization, stable radiation pattern, low cross-polarization, and stable peak realized gain. Most importantly, a compact size ($0.32\lambda_0 \times 0.32\lambda_0 \times 0.044\lambda_0$ at 1.915GHz) is remained to demonstrate its performance of convenient integration with other planar circuits. This compact broadband DRA can be employed in satellite, radar, and wireless communication fields.

REFERENCES

[1] S. Long, M. McAllister, and L. Shen, "The resonant cylindrical dielectric cavity antenna," *IEEE Trans. Antennas Propag.*, vol. AP-31, no. 3, pp. 406–412, May 1983.

[2] A. A. Kishk, Y. Yin, and A. W. Glisson, "Conical dielectric resonator antennas for wide-band applications," *IEEE Trans. Antennas Propag.*, vol. 50, no. 4, pp. 406–412, Apr. 2002.

[3] N. Yang and K. W. Leung, "Size reduction of omnidirectional cylindrical dielectric resonator antenna using a magnetic aperture source," *IEEE Trans. Antennas Propag.*, vol. 68, no. 4, pp. 3248–3253, Apr. 2020.

[4] N. Yang, K. W. Leung, and N. Wu, "Pattern-diversity cylindrical dielectric resonator antenna using fundamental modes of different mode families," *IEEE Trans. Antennas Propag.*, vol. 67, no. 11, pp. 6778–6788, Nov. 2019.

[5] K. W. Leung, X. S. Fang, Y. M. Pan, E. H. Lim, K. M. Luk, and H. P. Chan, "Dual-function radiating glass for antennas and light covers—Part II: Dual-band glass dielectric resonator antennas," *IEEE Trans. Antennas Propag.*, vol. 61, no. 2, pp. 587–597, Feb. 2013.

[6] D. Guha and C. Kumar, "Microstrip patch versus dielectric resonator antenna bearing all commonly used feeds: An experimental study to choose the right element.," *IEEE Antennas Propag. Mag.*, vol. 58, no. 1, pp. 45–55, Feb. 2016.

[7] R. Chair, A. A. Kishk, K. F. Lee, and C. E. Smith, "Wideband flipped staired pyramid dielectric resonator antennas," *Electron. Lett.*, vol. 40, no. 10, pp. 581–582, May 2004.

[8] Y. Gao, Z. Feng, and L. Zhang, "Compact asymmetrical T-shaped dielectric resonator antenna for broadband applications," *IEEE Trans. Antennas Propag.*, vol. 60, no. 3, pp. 1611–1615, Mar. 2012.

[9] A. Rashidian, L. Shafai, and D. M. Klymyshyn, "Compact wideband multimode dielectric resonator antennas fed with parallel standing strips," *IEEE Trans. Antennas Propag.*, vol. 60, no. 11, pp. 5021–5031, Nov. 2012.

[10] X. S. Fang, K.-P. Shi, and Y.-. X. Sun, "Design of the single-/dual-port wideband differential dielectric resonator antenna using higher order mode," *IEEE Antennas Wireless Propag. Lett.*, vol. 19, no. 9, pp. 1605-1609, Sep. 2020.

[11] R. Chowdhury, N. Mishra, M. M. Sani, and R. K. Chaudhary, "Analysis of a wideband circularly polarized cylindrical dielectric resonator antenna with broadside radiation coupled with simple microstrip feeding," *IEEE Access*, vol. 5, pp. 19478–19485, 2017.

[12] A. Buerkle, K. Sarabandi, and H. Mosallaei, "Compact slot and dielectric resonator antenna with dual-resonance, broadband characteristics," *IEEE Trans. Antennas Propag.*, vol. 53, no. 3, pp. 1020–1027, Mar. 2005.

[13] Nasimuddin and K. P. Esselle, "A low-profile compact microwave antenna with high gain and wide bandwidth," *IEEE Trans. Antennas Propag.*, vol. 55, no. 6, pp. 1880–1883, Jun. 2007.

[14] Y. Ge, K. P. Esselle, and T. S. Bird, "Compact dielectric resonator antennas with ultrawide 60%–110% bandwidth," *IEEE Trans. Antennas Propag.*, vol. 59, no. 9, pp. 3445–3448, Sep. 2011.

[15] Y. M. Pan and S. Y. Zheng, "A low-profile stacked dielectric resonator antenna with high-gain and wide bandwidth," *IEEE Antennas Wireless Propag. Lett.*, vol. 15, pp. 68–71, 2016.

[16] N. Mishra and R. K. Chaudhary, "A miniaturized ZOR antenna with enhances bandwidth for WiMAX applications," *Microw. Opt. Technol. Letter.*, vol. 58, no. 1, pp. 71–75, Jan. 2016.

[17] S. X. Ta and I. Park, "Low-profile broadband circularly polarized patch antenna using metasurface," *IEEE Trans. Antennas Propag.*, vol. 63, no. 12, pp. 5929–5934, Dec. 2015.

[18] N.-W. Liu, L. Zhu, W.-W. Choi, and X. Zhang, "A low-profile aperture-coupled microstrip antenna with enhanced bandwidth under dual resonance," *IEEE Trans. Antennas Propag.*, vol. 65, no. 13, pp. 1055–1061, Mar. 2017.

[19] R. K. Mongia, A. Ittibipoon, and M. Cuhaci, "Low profile dielectric resonator antennas using a very high permittivity material," *Electron. Lett.*, vol. 30, no. 17, pp. 1362–1363, Aug. 1994.

[20] N. Liu, L. Zhu, and W. Choi, "A Differential-fed microstrip patch antenna with bandwidth enhancement under operation of TM_{10} and TM_{30} modes," *IEEE Trans. Antennas Propag.*, vol. 65, no. 4, pp. 1607–1614, Apr. 2017.

[21] R. K. Mongia and A. Ittipiboon, "Theoretical and experimental investigations on rectangular dielectric resonant antennas," *IEEE Trans. Antennas Propag.*, vol. 45, no. 9, pp. 1348–1359, Sep. 1997.

[22] W. E. I. Liu, Z. N. Chen, and X. Qing, "Broadband low-profile L-probe fed metasurface antenna with TM leaky wave and TE surface wave resonances," *IEEE Trans. Antennas Propag.*, vol. 68, no. 3, pp. 1348–1355, Mar. 2020.

[23] J. Zhang, S. Yan, and G. A. E. Vandenbosch, "A miniature feeding network for aperture-coupled wearable antennas," *IEEE Trans. Antennas Propag.*, vol. 65, no. 5, pp. 2650–2654, May 2017.

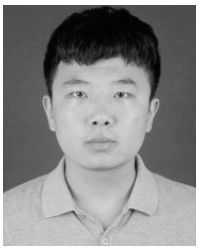

SHU-KUAN ZHAO was born in Shandong, China, in 1993. He received the B.S. degree in electronic and information engineering from Xidian University, Xi'an, China, in 2015, where he is currently pursuing the Ph.D. degree. His current research interests include planar integrated antennas and antenna array.

NENG-WU LIU (Member, IEEE) was born in Changde, China. He received the B.S. and M.E. degrees in electrical engineering from Xidian University, Xi'an, China, in 2012 and 2015, respectively, and the Ph.D. degree from the University of Macau, Macau, China, in 2017.

He is currently an Associate Professor with Xidian University. His current research interests include wideband antennas and circularly polarized antennas. He serves for the Editorial Board of several journals, including *IET Microwaves, Antennas and Propagation*, IEEE Access, and *IET Electronics Letters*. He has also served on the Review Board of many journals, including the IEEE Transantions on Antennas and Propagation, IEEE Antennas and Wireless Propagation Letters, and IEEE Access.

QIANG CHEN (Senior Member) received the B.E. degree from Xidian University, Xi'an, China, in 1986, and the M.E. and D.E. degrees from Tohoku University, Sendai, Japan, in 1991 and 1994, respectively. He is currently a Chair Professor with the Electromagnetic Engineering Laboratory, Department of Communications Engineering, Faculty of Engineering, Tohoku University.

GUANG FU received the B.S. and M.S. degrees in electromagnetic field and microwave technology from Xidian University, in 1984 and 1991, respectively. He became a Professor at Xidian University, in 2001. His current research interests include theory and engineering of antenna and antenna array.

XIN-PENG CHEN was born in Fujian, China, in 1995. He received the B.S. and M.E. degrees in electronic and information engineering from Xidian University, Xi'an, China, in 2017 and 2020, respectively. His current research interests include wide-band antenna and microstrip antenna.